Influence of Extreme Velocities on Dynamic Cavity Expansion

by

Kelsey Lynn Wittels

B.S., Civil and Environmental Engineering
University of California Los Angeles, 2015

Submitted to the Department of Civil and Environmental Engineering
in partial fulfillment of the requirements for the degree of

Master of Engineering in Civil and Environmental Engineering

at the

MASSACHUSETTS INSTITUTE OF TECHNOLOGY

June 2017

Author .... Signature redacted .....
Department of Civil and Environmental Engineering
May 12, 2017

Certified by.. Signature redacted .....
Tal Cohen
Assistant Professor of Civil and Environmental Engineering
Thesis Supervisor

Accepted by ... Signature redacted .....
Jesse Knoll
Professor of Civil and Environmental Engineering
Chair, Graduate Program Committee

Influence of Extreme Velocities on Dynamic Cavity Expansion

by

Kelsey Lynn Wittels

Submitted to the Department of Civil and Environmental Engineering
on May 12, 2017, in partial fulfillment of the
requirements for the degree of
Master of Engineering in Civil and Environmental Engineering

Abstract

Cavitation can broadly be described as the unstable expansion of an empty void in a body, usually occurring when loads on the body reach a critical level. In this thesis, dynamic cavity expansion (DCE) in solids is of particular interest. Cavity expansion has been studied extensively under quasi-static and dynamic loading conditions. However, the behavior of cavitation fields with extreme dynamic expansion velocities have little been studied, especially in materials without a definite yield point. In this thesis, DCE in a hardening elastoplastic medium is considered under extreme velocities. Two nonlinear differential equations are used to describe the steady-state expansion. Using numerical integration, this system is solved to explore the behavior under extreme expansion velocities. By gradually increasing the expansion velocities, we find that a singularity occurs in the governing system, indicating a shock wave emerging and propagating through the material. With this limit velocity of the material known, further characteristics of the material can be described and investigated.

Thesis Supervisor: Tal Cohen
Title: Assistant Professor of Civil and Environmental Engineering

Acknowledgments

This thesis would not have been possible without the help from many individuals. First and foremost, I would like to thank my adviser, Tal, for her guidance and patience with me while I pursued this topic. I would never have been introduced (and especially encouraged) to pursue a problem in this domain without you. Secondly, I am very much in gratitude to my other professors at MIT for my success; John and Gordana, thank you for sculpting an incredible program. I am also grateful for the camaraderie and support from all of my classmates of "M'Eng". It has been a pleasure to work alongside you all and I wish you the best luck in your future endeavors. Finally, and possibly most importantly, thank you to Mom, Dad, Anja, Mason and Erik for your everlasting support. Your encouragement has helped me to become the person I am today and I know many of my accomplishments are due to the loving background I come from.

Contents

List of Figures

Chapter 1

Introduction

To begin, consider an infinite solid medium, such as a metal. Inside this otherwise uniform material there exists a void or a defect, which can be called a cavity. The cavity is assumed to be very small compared to the material in which it exists; therefore, when looking at the cavity, the material outside of it is considered infinite. The presence of this cavity is inconsequential until the material is subjected to a load. As seen in Figure 1-1, the loading applied to a cavity can be considered as an internal pressure or an external tension.

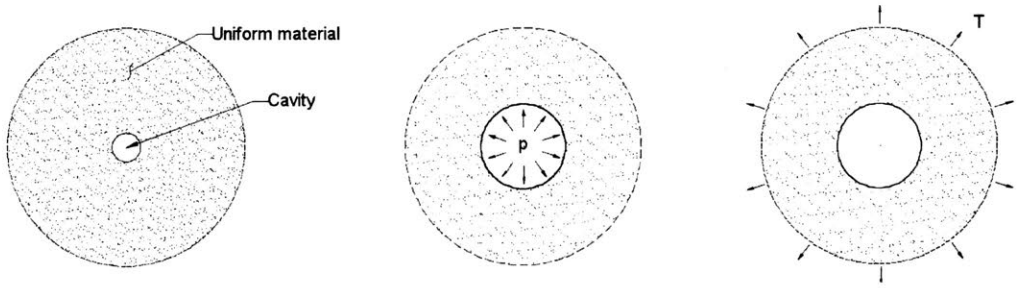

(a) Initial State (b) Internal pressure, P (c) External tension, T

Figure 1-1: Cavity in an infinite medium subject to different loading conditions

This type of loading can occur due to several different conditions, such as growth, drying, or fracture of the material. Once the material is loaded, the presence of the cavity creates a state in which the material is no longer in equilibrium. Figure 1-2 shows the general behavior of the material subjected to loads. When the load applied is increased, the radius of the cavity also increases. However, there is a critical load

that causes the radius of the cavity to expand spontaneously. This asymptotic limit is known as the cavitation pressure. A constant load applied at this critical level causes a steady-state expansion of the cavity.

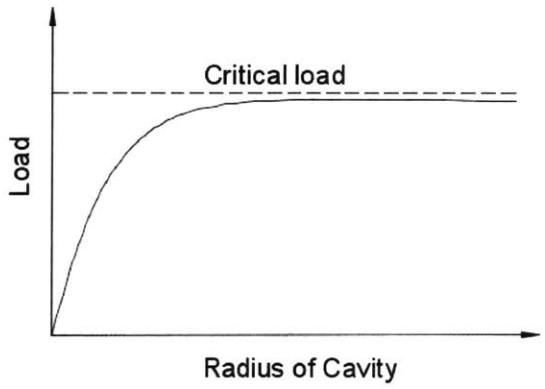

Figure 1-2: Loading applied to a cavity and corresponding radius

Cavity expansion is studied primarily under two different loading conditions: quasi-static and dynamic. Quasi-static loadings consider the load to be increased very slowly and allow for the system to maintain equilibrium. However, the material reaches a limit where this type of loading can exist, as shown by the critical load in Figure 1-2. Above this critical load, equilibrium cannot be achieved and dynamic cavity expansion (DCE) occurs. Here, if the load is constant, the cavity expands at a constant rate. Dynamic loadings can occur due to impacts, blasts, and ballistic penetration. The study of cavitation fields is commonly used to model these phenomena in materials. In this thesis, cavitation fields are studied under dynamic expansion and pushed until the presence of a shock wave is observed.

1.1 Motivation

Nearly all materials are made with some imperfections and thus cavities are present. Dynamic cavity expansion (DCE) has been shown to occur in many different materials, including metals, soils, and soft materials. For example, cavitation occurs in metals subjected to penetration [14], soils subjected to large compression loads induced by pile driving [8], and soft tissues such as those in the brain as a result of

impacts or explosions [17].

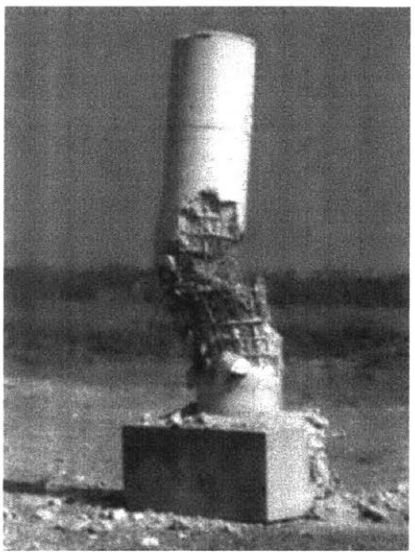

Figure 1-3: Column subjected to a blast load. Reproduced from Yi, et al [19]

Moreover, the study of DCE has a broad range of applications. A main motivation for studying DCE is in the significance to protective structures. With better understanding of how cavities expand under dynamic loading, structures can be designed more appropriately for blast mitigation and severe impacts. One example of this is shown in Figure 1-3, where a bridge pier has failed as the result of a blast load test. Another application is in the design of protective armor in order to protect against bullet penetration. Figure 1-4 shows the penetration of an aluminum armor plate. It can be seen that initially there was no hole in the material yet when the penetration occurs, a hole rapidly grows to a finite size in a very small time interval.

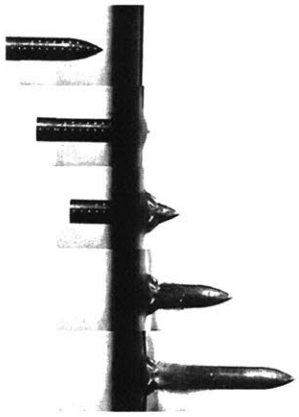

Figure 1-4: Bullet penetrating a metal object. Reproduced from Borvik, et al [5]

Furthermore, with continued research, the effects of underground explosions, planetary impacts, soil liquefaction, and volcanic eruptions can be better understood and predicted. A benchmark solution in this field can also be used to describe the governing systems associated with the above applications. For example, if penetration energy is better understood, protective structures and armor can be designed to withstand this energy. With further understanding, energy dissipation levels of different materials may also be quantified. This could lead to new understanding of the most optimal materials for blast, impacts, and protective design. Similarly, a benchmark solution would shed light on characteristic expansion velocities which would

also allow for materials to be used at their greatest capacity.

Finally, in all of these situations, shock waves may appear. Shock waves may occur in materials due to earthquakes, blasts, and planetary impacts. With increased knowledge of shock wave behavior in solids, materials can be designed to mitigate, or even potentially exploit the power of shock waves for increased energy dissipation and enhanced performance.

1.2 History of the Field

The study of cavitation fields erupted during WWII in response to the need to predict material response to penetration. Bishop, Hill, and Mott [2] established a precedent in this field by devising a cavitation-based method to predict hardness of a material by indentation. By studying the load at which a conical indentation tool penetrates a semi-infinite block of ductile material, they find that there is a critical resisting load and predict that it is equal to the critical cavitation pressure (as shown in Figure 1-2). They developed the first analytical models for penetration mechanics which predominantly focused in the quasi-static cavitation setting.

As the study of cavitation furthered, cavity expansion was explored for various geometries. The study of cavitation in thin sheets began during WWII with the work of G.I. Taylor [18], Hill [13], and Bethe in unpublished work [1]. Significant study has been conducted for spherical geometries by researchers such as Hunter [15], Forrestal and Luk [12], and Durban and Baruch [9]. Cylindrical cavity expansion is also of considerable interest in the geotechnical field where pile driving phenomena and penetration tests can be analytically modeled by an internally pressurized cavity [8].

Once solutions became apparent in the quasi-static setting, the behavior of cavitation fields under dynamic loadings were explored. Hopkins [14] and Bland [4] applied techniques commonly used in fluid dynamics to understand dynamic deformations in solids. In a previous work, Bland also hypothesized how to treat shock waves in elastic solids [3]. Since then, a considerable amount of work has been put into solving the

system for dynamic cavity expansion. Durban and Baruch [9] formulated governing nonlinear differential equations and numerical results for spherical cavity expansion in an elastoplastic medium. Following this, studies were expanded to Drucker-Prager solids [10] and a pressure sensitive medium [11]. A comprehensive overview of the work in this field is given by Masri [16].

In all of the previously mentioned work, cavity expansion studies were limited to moderate velocities. Each of these studies limited the expansion velocity to cases where it was much smaller than the speed of sound. For the first time, the influence of shock waves in dynamic cavity expansion is investigated by Cohen [6]. In Cohen's paper, high velocity cavitation fields are explored and the subsequent emergence of shock waves in the material is described. However, Cohen's study is limited to materials with a definite yield point. This thesis builds predominantly on the work previously published by Masri and Durban [16] and their formulation for dynamic spherical cavity expansion in an elastoplastic compressible Mises solid, as well as on the work previously published by Cohen [16] for extreme expansion velocities.

1.3 Scheme

The goal of this thesis is to expand on the current knowledge of cavitation fields into the domain of large expansion velocities in materials with no definite yield point. In order to accomplish this, the work published by Masri and Durban [16] is used as a reference to formulate the governing system in Chapter 2. An overview of the cavitation field governing system is given in Section 2.1. Here, a synthesis of the boundary conditions are described and the governing equations are derived. Next, in Section 2.2, a numerical integration technique is chosen to solve the system. Once the system has been integrated, the results are then compared to existing literature in Section 2.3 to confirm accuracy. Next, since the model is validated by comparison to previous results, it can be used to expand the study for increasing velocities.

Chapter 3 focuses on the behavior of the system is investigated under increasing velocities. The dynamic expansion velocity is increased until discontinuities occur in

the system. In Section 3.2, the limit of the system, as shown by a singularity in the integration, is investigated. This singularity is then described by the presence of a shock wave in Section 3.3.

Finally, the thesis is concluded in Chapter 4 with a discussion of further applications of this study. Future work is divided into three sections: work that can be completed immediately (Section 4.1), in the near future (Section 4.2), and further on (Section 4.3).

Chapter 2

Dynamic Expansion of a Spherical Cavity

2.1 Problem Formulation

In order to consider the behavior of a material under dynamic cavity expansion, the derivation from Masri and Durban [16] was followed and a complete derivation can be found there. In brief, a spherical cavity is assumed to be situated in an infinite medium. An internal constant pressure, p, is applied causing the cavity to expand with constant velocity and under steady-state conditions. The material is assumed to be expanding under self-similar conditions and the material response was modeled by J_2 flow theory plasticity, accounting for a compressible elastic branch and logarithmic strain components.

The material is considered to be unbounded and spherically symmetric. As seen in Figure 2-1, the field can be defined in a spatial spherical coordinate system (R, θ, ϕ) where the origin is located at the center of the cavity. The nondimensional radial coordinate is defined as $\xi = \frac{R}{A}$, where R is the Eulerian radial coordinate and A is the instantaneous radius of the cavity.

Since the material is infinite, the remote boundary at infinity can be considered undeformed and stress free, and thus does not experience the effects of the cavitation field. Where the cavitation field meets the undeformed and stress-free portion of the

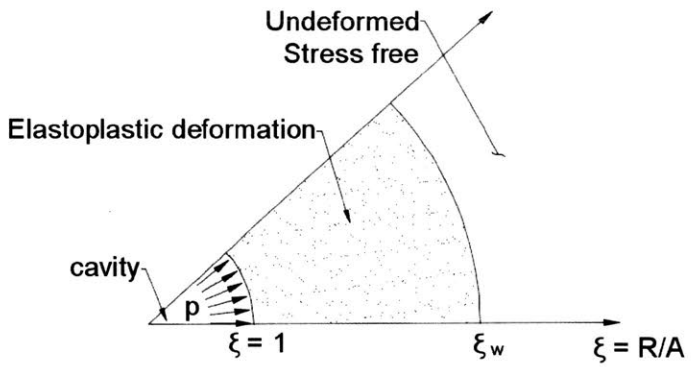

Figure 2-1: Schematic of a cavity in self-similar field under dynamic expansion. ξ represents the nondimensionalized radial coordinate and p is the applied pressure.

material is called the rigid elastic interface, or the wave front, ξ_w. However, at the cavity wall, where $\xi = 1$, the cavitation pressure is pushing out on the material, causing deformation.

The active Cauchy stress components are σ_r, σ_θ, and σ_ϕ, where in the spherically symmetric case, $\sigma_\theta = \sigma_\phi$. The radial equation of motion can then be written as

$$\frac{d\sigma_r}{dR} + \frac{2}{R}(\sigma_r - \sigma_\theta) = \rho\ddot{R} \tag{2.1}$$

where ρ is the density and a superimposed dot indicates differentiation with respect to time. To complete the description of the field, conservation of mass and constitutive relations are taken into consideration. The effective stress, σ, and the hydrostatic stress, σ_h, can be described using the following relations:

$$\sigma = \sigma_\theta - \sigma_r \tag{2.2}$$

$$\sigma_h = \frac{1}{3}(\sigma_r + 2\sigma_\theta) = \sigma_r + \frac{2}{3}\sigma \tag{2.3}$$

where σ_r is the radial stress.

Similarly, for the spherically symmetric field, the J_2 flow theory formulation can be simplified to the following Eulerian strain rates:

$$\dot{\epsilon}_r = \frac{1-2\nu}{E}\dot{\sigma}_r - \frac{2\nu}{E}\dot{\sigma} - \dot{\epsilon}_p \tag{2.4}$$

$$\dot{\epsilon}_\theta = \frac{1-2\nu}{E}\dot{\sigma}_r - \frac{1-\nu}{E}\dot{\sigma} + \frac{1}{2}\dot{\epsilon}_p \tag{2.5}$$

where ϵ denotes strain, ν is the Poisson ratio, E is the elastic modulus, and ϵ_p is the effective plastic strain, which is a known function of σ. With ν and E as constants and ϵ_p as a function of σ, the two stress components, σ_r and σ, can now be used to describe the system. The stress components are then rewritten as nondimensionalized with respect to the elastic modulus, $(\Sigma_r, \Sigma) = (\sigma_r, \sigma)/E$.

Steady-state expansion assumes $\dot{A}$ is constant, so the only independent variable is $\xi = \frac{R}{A}$. Using this similarity relation outlined by Durban and Fleck [10], two ordinary nonlinear differential equations can be derived for the governing system:

$$\beta\Sigma_r' + \frac{\beta}{2}\Sigma' + \frac{1}{2}\epsilon' = \frac{1}{\xi}(1 - e^{-\frac{\beta}{2}\Sigma + \frac{3}{2}\epsilon}) \tag{2.6}$$

$$\Sigma_r' - \frac{2}{\xi}\Sigma = m^2\xi^2(\beta\Sigma_r' + \beta\Sigma' - \epsilon')e^{-3\beta\Sigma_r - \beta\Sigma - 3\epsilon} \tag{2.7}$$

where a superimposed prime indicates the variable is differentiated with respect to ξ. In the above equations, β represents the elastic-compressibility parameter, which is a function of the material's Poisson ratio, $\beta = 1 - 2\nu$. The variable ϵ represents the total strain, $\epsilon = \Sigma + \epsilon_p$. Again, the variable ϵ_p represents the effective plastic strain. The Ramberg-Osgood Power Law is used to represent strain hardening of a material without a definite yield point. The equivalent plastic strain is given from the uniaxial tension test where ϵ_p is defined as $\epsilon_p = K\Sigma^\alpha$ where K and α are material parameters.

Additionally, note the presence of the variable m in equations (2.6) and (2.7). Here, m represents the nondimensional cavity expansion velocity, which is defined as the ratio between the cavity expansion velocity ($\dot{A}$) and the longitudinal wave speed in a linearly elastic rod ($\sqrt{E/\rho_0}$).

$$m = \frac{\dot{A}}{\sqrt{\frac{E}{\rho_0}}} \tag{2.8}$$

Quasi-static expansion occurs when $m = 0$. Masri and Durban [16] use the value of $m = 0.35$ for dynamic expansion and thus this value will be used in the next section

to compare results.

Once equations (2.6) and (2.7) are solved for, radial velocity and density may also be determined because they are known functions of these stresses. Radial velocity is found by taking a time derivative of the radial coordinate, ξ, and can be written as $V = \dot{R}/\dot{A}$. The reference density of the undeformed stress-free state is indicated by ρ_0 and thus the density ratio is written as ρ/ρ_0. In terms of stresses, radial velocity and the density ratio can be written, respectively, as

$$V = \xi(1 - e^{-\phi}) \qquad \text{where} \qquad \phi = (1+\nu)\Sigma + \frac{3}{2}\epsilon_p \tag{2.9}$$

$$\frac{\rho}{\rho_0} = e^{-\Theta} \qquad \text{where} \qquad \Theta = \beta(3\Sigma_r + 2\Sigma) \tag{2.10}$$

2.2 Numerical Integration

To sum up, the governing system can be described by a system of four equations, (2.6), (2.7), (2.9), (2.10) and four unknown field variables (Σ_r, Σ, V, $\frac{\rho}{\rho_0}$). Since V and $\frac{\rho}{\rho_0}$ can be described using the closed-form relations described in equations (2.9) and (2.10), the two ordinary nonlinear differential equations, (2.6) and (2.7), are integrated numerically and thus are rewritten in the following matrix form:

$$\begin{bmatrix} \beta & \frac{1}{2}(\beta + \frac{d\epsilon}{d\Sigma}) \\ \beta - \frac{1}{m^2\xi^2} e^{3\beta\Sigma_r + \beta\Sigma + 3\epsilon} & \beta - \frac{d\epsilon}{d\Sigma} \end{bmatrix} \begin{Bmatrix} \Sigma_r' \\ \Sigma' \end{Bmatrix} = \begin{bmatrix} \frac{1}{\xi}(1 - e^{\frac{-\beta}{2}\Sigma + \frac{3}{2}\epsilon}) \\ \frac{-2}{m^2\xi^3}\Sigma e^{3\beta\Sigma_r + \beta\Sigma + 3\epsilon} \end{bmatrix} \tag{2.11}$$

where the first matrix is the coefficient matrix.

We can now proceed to formulate boundary conditions. Since the cavitation field meets the undeformed portion of the material at the wave front, ξ_w, stresses can be assumed to be zero there. At the cavity wall, where the nondimensionalized radial coordinate is equal to one, the effective stress goes to infinity and the radial stress is equal to the cavitation pressure, P_c, which is also nondimensionalized with respect to

the elastic modulus. The boundary conditions can be written as:

$$\xi = \xi_w : \quad \Sigma_r = 0, \quad \Sigma = 0, \quad (\rho = \rho_0, \quad V = 0) \tag{2.12}$$

$$\xi = 1 : \quad \Sigma_r = -P_c, \quad \Sigma \to \infty, \quad (\rho \to 0, \quad V = 1) \tag{2.13}$$

Since cavitation pressure is determined by the solution, integration is performed beginning at the wave front ($\xi = \xi_w$) and is stepped backwards up to the cavity wall ($\xi = 1$). However, since all field variables vanish at the remote boundary, this introduces a trivial solution. To overcome this, the first step of the integration was calculated by requiring that the determinant of the coefficient matrix in equation (2.11) vanishes to find $\xi = \xi_w$. This introduces an unknown constant into the integration and then a shooting method for the value of the constant must be used until the boundary conditions are satisfied at both ends.

Next, in order to separate and solve for the stress components, Σ' and Σ_r', Cramer's Rule was used. The Runge-Kutta-Merson 5th Order Approximation was chosen for increased accuracy from earlier devised results. An overview of the Runge-Kutta-Merson method can be found in Appendix A. The step of the integration along ξ was reduced until the solution was convergent. The calculated values of Σ and Σ_r can then be used in equations (2.9) and (2.10) to solve for the velocity and the density of the system along ξ.

2.3 Confirmation of Results

In order to properly compare the results with Masri and Durban [16], the integration was performed with the properties of Aluminium 7075-T6. For this metal, the following properties were used:

$$\epsilon_p = 3.94 * 10^{21}\Sigma^{10.9}, \quad \nu = 0.32, \quad \rho_0 = 2700\frac{kg}{m^3}, \quad E = 72.4Gpa$$

where ϵ_p is of the form $\epsilon_p = K\Sigma^{\alpha}$.

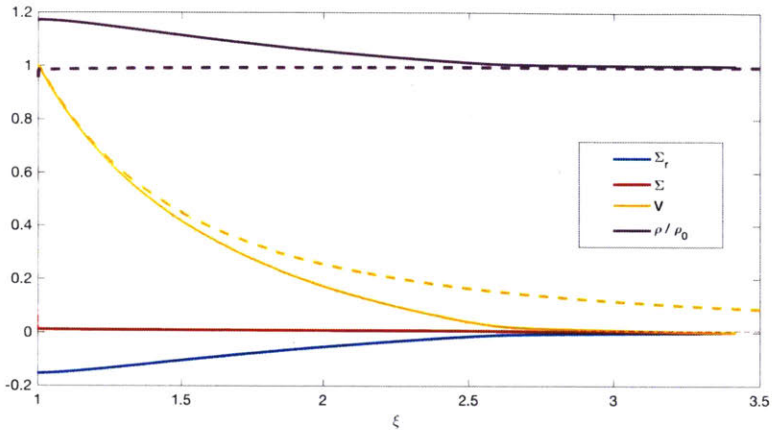

Figure 2-2: Reproduced radial profiles of essential field variables for AL 7075-T6. Values for m = 0.35 are shown in a solid line and values for m = 0 are shown with dotted lines.

The curves for the effective stress, Σ, radial stress, Σ_r, velocity, V, and density ratio, $\frac{\rho}{\rho_0}$ were then plotted against the radial coordinate, ξ and can be seen in Figure 2-2. The results that were published by Masri and Durban [16] are shown for comparison in Figure 2-3.

Figure 2-2 shows the profile of a material from the cavity wall to the elastic wave front, which in this case $\xi_w = 3.42$. As expected, the effective stress (Σ) is zero at the wave front and tends toward infinity just as it approaches the cavity wall. The tendency towards infinity at the cavity wall is not well seen because the boundary layer near the wall is extremely small [11]. The radial stress (Σ_r) also begins at zero but decreases until it reaches a finite value at the cavity wall. The value of radial stress at the cavity wall is finite, as expected. The density ratio arrives at a peak value near the cavity wall and then decreases until the material is undeformed and subsequently the ratio reaches 1 at the wave front. Finally, the velocity profile is shown for the quasi-static solution of $m = 0$ and the dynamic solution of $m = 0.35$. It can be seen that the gradient of the velocity profile increases with an increase in m.

It is notable that for this thesis, the results of Masri and Durban [16] were able to be successfully reproduced. Since the results here have been validated, the numerical integration system can be used to expand on the previous study.

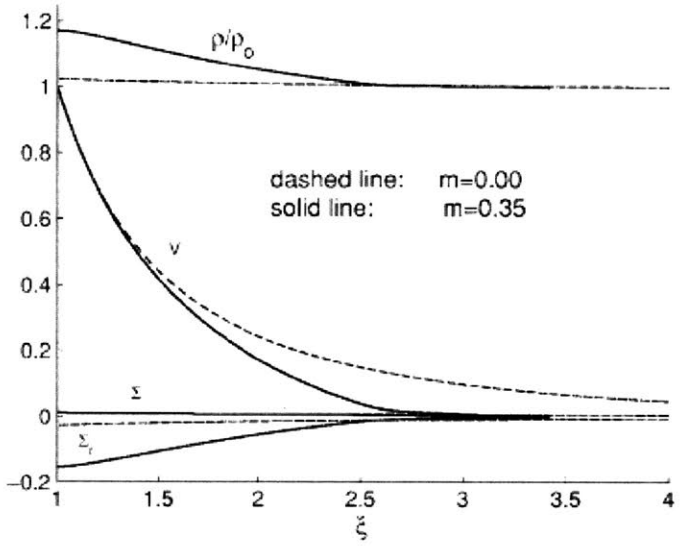

Figure 2-3: Results from Masri and Durban (2005) for 'Radial Profiles of essential field variables for AL 7075-T6'

Chapter 3

Expanding Velocities

In the preceding chapter, the system was integrated for a dynamic cavity expansion velocity of $m = 0.35$, or in physical quantities, it was expanding at a rate of 1812 m/s. Next, the system is investigated under more extreme velocities. The same equations and methodology are used but the cavity expansion velocity, m, is adjusted. The value of m is increased until a singularity occurs.

3.1 Behavior

The influence of dynamic cavity expansion velocity on the radial velocity profile is shown in Figure 3-1 for $m = 0.1$, 0.35, 0.5, and 0.6.

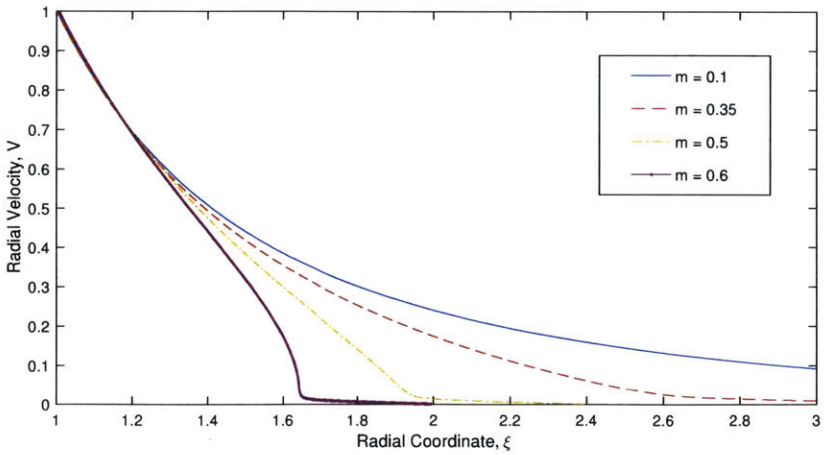

Figure 3-1: Influence of m on radial velocity

It is notable that with the increase in the value of m, the local gradient of the curve increases and more drastically. Additionally, as the value of m is increased, the curve for the radial velocity moves closer and closer to the cavity wall. Importantly, in the range of $\xi = 1.6 - 1.7$, the curve for $m = 0.6$ starts to exhibit extreme changes in the local gradients. An extreme localized gradient zone occurs, and then the curve returns to the expected behavior as it approaches an asymptotic limit at $\xi = 1$.

Figure 3-2 shows the cavitation pressure, P_c as a function of cavity expansion velocity, m. It can be seen that as the expansion velocity increases, the cavitation pressure increases disproportionally.

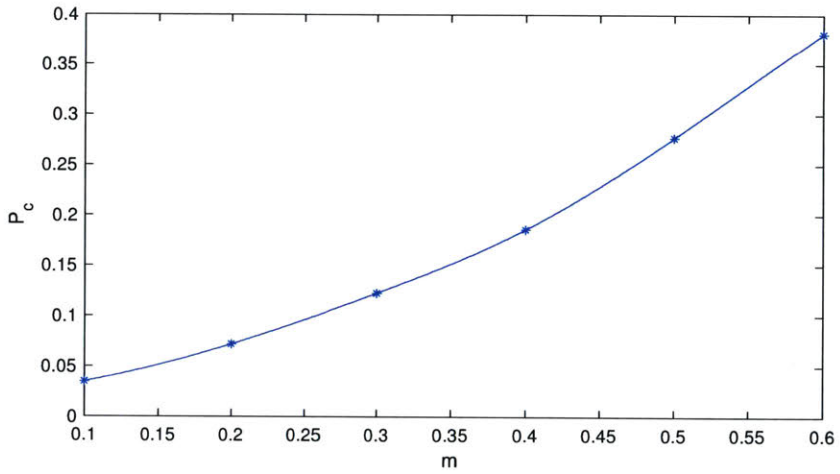

Figure 3-2: Cavitation pressure as a result of increasing expansion velocities. A spline interpolation is used for the curve fitting line.

3.2 Singularity

For the given system, increasing the value of m was attempted. Previously published papers are usually limited to values in the range of $m < 0.4$. In expanding the values of m beyond $m = 0.6$, the localized gradient zone becomes even more extreme. Thus, $m \approx 0.6$ appears to be a limit for this material's expansion velocity. At values greater than $m = 0.6$, the numerical integration failed, indicating a mathematical singularity may occur here. If graphed, the behavior of curves for $m > 0.6$ start to become discontinuous, jumping abruptly at finite values to extremes in both positive

and negative values. Additionally, no refinement of the numerical integration step changes this abrupt behavior.

This unusual behavior likely can be explained by one of two things: 1) An issue in the numerical integration, or 2) the response of the material. In order to evaluate this, recall equation (2.11) from Chapter 2 that defines the governing system:

$$\begin{bmatrix} \beta & \frac{1}{2}(\beta + \frac{d\epsilon}{d\Sigma}) \\ \beta - \frac{1}{m^2\xi^2} e^{3\beta\Sigma_r + \beta\Sigma + 3\epsilon} & \beta - \frac{d\epsilon}{d\Sigma} \end{bmatrix} \begin{Bmatrix} \Sigma_r' \\ \Sigma' \end{Bmatrix} = \begin{bmatrix} \frac{1}{\xi}(1 - e^{\frac{-\beta}{2}\Sigma + \frac{3}{2}\epsilon}) \\ \frac{-2}{m^2\xi^3} \Sigma e^{3\beta\Sigma_r + \beta\Sigma + 3\epsilon} \end{bmatrix}$$

The solution was obtained by finding the determinant of the coefficient matrix. When the determinant is equal to zero, there is more than one possible solution. Therefore, inspection of the determinant of the system under these extreme velocities is necessary. Figure 3-3 portrays the value of the determinant with respect to the radial coordinate. The curves have been truncated if the value of the determinant is less than or equal to zero. The limit expansion velocity of this material before the determinant goes below zero appears to occur around $m \approx 0.6$.

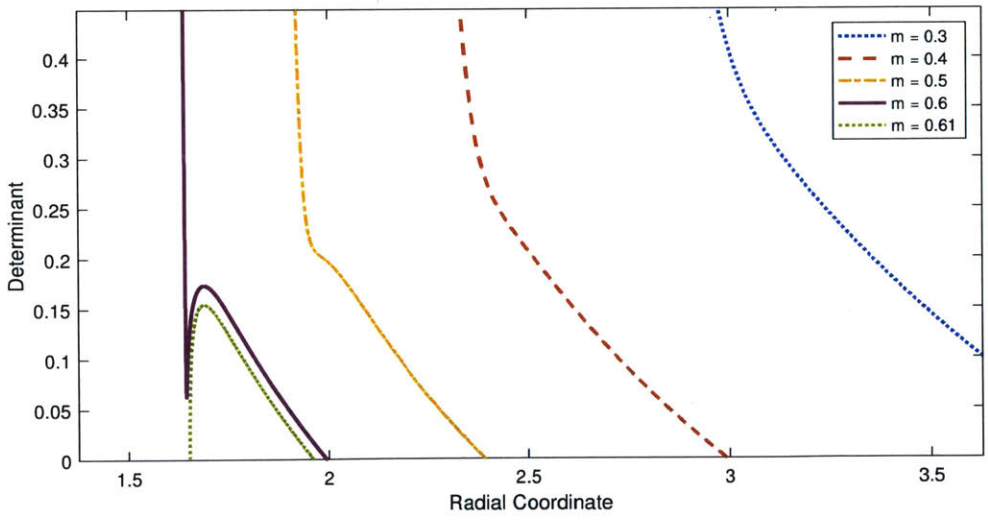

Figure 3-3: Behavior of the determinant under different expansion velocities.

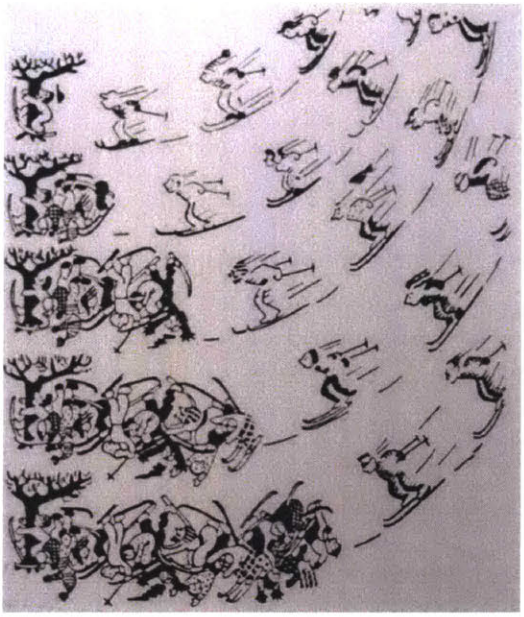

Figure 3-4: Cartoon depiction of a shock wave. Reproduced from Courant and Friedrichs [7].

For expansion velocities greater than $m = 0.6$, the value of the determinant goes below zero. However, when the determinant of the system is equal to zero, the solution of the system is singular and multiple solutions are permitted. This leads to a conclusion that, at this point, discontinuity of the field variables is permitted. This condition exists physically when a shock wave is propagating through a material.

To intuitively explain the circumstances that lead to the appearance of discontinuities in a material, a cartoon depiction of a metaphorical shock wave is shown in Figure 3-4. The skiers are following each other extremely closely and moving very fast. As soon as something occurs to the skier in front, the others are moving too quickly and closely and do not have enough time to react. Thus, the collision propagates back through the line of skiers at a velocity that is dictated by the response time of the skiers. Analogously, in our material at extreme velocities, the cavitation is expanding at a supersonic speed and a plastic shock propagates at a velocity that is dictated by the nonlinear response of the material.

3.3 Shock Wave

Once the system becomes singular, different values for Σ_r, Σ, V, and $\frac{\rho}{\rho_0}$ exist on either side of the shock. The governing system must then be replaced by finite relations, or jump conditions. Two fundamental conditions are the Hugonoit jump conditions, which impose conservation of mass and conservation of momentum on either side of the shock. In terms of variables used in this thesis, these jump conditions can be

written using [6] as:

$$\left[\!\left[\frac{\rho}{\rho_0}(\xi_w - V)\right]\!\right] = 0 \tag{3.1}$$

$$\left[\!\left[\Sigma_r + m^2\frac{\rho}{\rho_0}(\xi_w - V)V\right]\!\right] = 0 \tag{3.2}$$

where the brackets $[\![...]\!]$ indicate the relation is true on each side of the shock.

A third condition is the continuity of radial displacement across the shock, which in this case translates to the continuity of circumferential strain [6], and can be written as:

$$\left[\!\left[\beta\Sigma_r + (1-\nu)\Sigma + \frac{1}{2}\epsilon_p\right]\!\right] = 0 \tag{3.3}$$

A final condition requires that the determinant of the coefficient matrix is equal on both sides of the shock:

$$\left[\!\left[\beta m^2\xi^2 - \frac{\frac{d\epsilon}{d\Sigma} + \beta}{3\frac{d\epsilon}{d\Sigma} - \beta}e^{3\beta\Sigma_r + \beta\Sigma + 3\epsilon}\right]\!\right] = 0 \tag{3.4}$$

We now have four equations (3.1) - (3.4) to describe the material on either side of the shock. Integration has already been completed close to one side of the shock, where the material properties V_1, $\frac{\rho_1}{\rho_0}$, Σ_{r1} and Σ_1 are known. Using these jump conditions, we are then left with four unknowns on the other side of the shock: V_2, $\frac{\rho_2}{\rho_0}$, Σ_{r2} and Σ_2. These values can then be solved for and thus a complete numerical solution can be compiled despite the presence of discontinuities.

Chapter 4

Concluding Remarks and Future Work

In summary, dynamic spherical cavity expansion in a compressible Mises solid has been investigated in this thesis. First, cavitation fields are studied under known velocities and then expanded to greater velocities. However, with the increase of expansion velocity, the numerical integration fails and a singularity appears in the governing system of equations. Once this singularity occurs, a shock wave is shown to be propagating through the material.

In a continuation of the work presented here, the field of shock wave propagation in solids holds many more questions. The behavior of shock waves in solids is relatively undeveloped and therefore invites potential future work. This thesis presents potential work that can be classified into three categories: work that can be done immediately (completion of jumping the shock), in the near future (response of other geometries) and further on (structural design applications).

4.1 Jump Conditions Across the Shock

A task that is currently being undergone is solving for the field variables across the shock. Hugonoit jump conditions have been applied and the new governing system is being solved. Once this is complete, it will be possible to describe the entire

cavitation field at extreme velocities, despite discontinuities in the material. Further characteristics of materials experiencing shock waves can then investigated

4.2 Different Geometries

Furthermore, dynamic cavity expansion can be investigated in other geometries. While shock waves have been studied in spherically symmetric geometries, future work will potentially include expanding this study and inspecting how geometry influences cavitation.

4.3 Applications

Finally, in a more extensive future study, the applications of this work to the physical world have the potential for an incredible impact. By further studying and developing analytical tools for describing shock wave propagation in solids, the way we design structures may be transformed, especially for blast impacts. Shock waves are known to occur following explosions, yet the response of solid materials is little understood. Future questions include: How do shock waves propagate through known structural materials? Could the energy dissipated through plastic deformation in a shock wave reduce the structural damage following an event? What are the benefits and downsides of designing a material to induce a shock wave?

Appendix A

Runge-Kutta-Merson 5th Order Approximation

$$\left\{\begin{array}{l} \frac{\delta x}{\delta t} = g(t,x,y) \\ \frac{\delta y}{\delta t} = f(t,x,y) \end{array}\right\} \quad \text{where} \quad \left\{\begin{array}{l} x_{k+1} = x_k + \frac{1}{6}(m_1 + 4m_4 + m_5) + O(h^5) \\ y_{k+1} = y_k + \frac{1}{6}(y_1 + 4y_4 + y_5) + O(h^5) \end{array}\right\}$$

h = time step and O = error term

$$\left\{\begin{array}{l} m_1 = h * g(t_k, x_k, y_k) \\ k_1 = h * f(t_k, x_k, y_k) \end{array}\right\}$$

$$\left\{\begin{array}{l} m_2 = h * g(t_k + \frac{1}{3}h, x_k + \frac{1}{3}m_1, y_k + \frac{1}{3}k_1) \\ k_2 = h * f(t_k + \frac{1}{3}h, x_k + \frac{1}{3}m_1, y_k + \frac{1}{3}k_1) \end{array}\right\}$$

$$\left\{\begin{array}{l} m_3 = h * g(t_k + \frac{1}{3}h, x_k + \frac{1}{6}(m_1 + m_2), y_k + \frac{1}{6}(k_1 + k_2)) \\ k_3 = h * f(t_k + \frac{1}{3}h, x_k + \frac{1}{6}(m_1 + m_2), y_k + \frac{1}{6}(k_1 + k_2)) \end{array}\right\}$$

$$\left\{\begin{array}{l} m_4 = h * g(t_k + \frac{1}{2}h, x_k + \frac{1}{8}(m_1 + 3m_3), y_k + \frac{1}{8}(k_1 + 3k_3)) \\ k_4 = h * f(t_k + \frac{1}{2}h, x_k + \frac{1}{8}(m_1 + 3m_3), y_k + \frac{1}{8}(k_1 + 3k_3)) \end{array}\right\}$$

$$\left\{\begin{array}{l} m_5 = h * g(t_k + h, x_k + \frac{1}{2}(m_1 - 3m_3 + 4m_4), y_k + \frac{1}{2}(k_1 - 3k_3 + 4k_4)) \\ k_5 = h * f(t_k + h, x_k + \frac{1}{2}(m_1 - 3m_3 + 4m_4), y_k + \frac{1}{2}(k_1 - 3k_3 + 4k_4)) \end{array}\right\}$$

Bibliography

[1] H. A. Bethe. An attempt at a theory of armor penetration. Ordnance Laboratory Report, Frankford Arsenal, 1941.

[2] R. F. Bishop, R. Hill, and N. F. Mott. The theory of indentation and hardness tests. *The Proceedings of the Physical Society*, 57(321):147–159, 1945.

[3] D. R. Bland. *Second-Order Effects in Elasticity, Plasticity and Fluid Dynamics.* International Symposium, Haifa, Israel. Jerusalem: Pergamon Press: Oxford, 1962.

[4] D. R. Bland. Dilational waves and shocks in large displacement isentropic dynamic elasticity. *Journal of Mech. Phys. Solids*, 12:245–267, 1964.

[5] T. Brvik, M. J. Forrestal, and T. L. Warren. Perforation of 5083-h116 aluminum armor plates with ogive-nose rods and 7.62 mm apm2 bullets. *Experimental Mechanics*, 50(959), 2010.

[6] Tal Cohen, Rami Masri, and David Durban. Shock waves in dynamic expansion. *Journal of Applied Mechanics*, 77(041009):1–8, July 2010.

[7] Richard Courant and K.O. Friedrichs. *Supersonic Flow and Shock Waves.* Springer Science Business Media, 1976.

[8] D. Durban and P. Papanastasiou. Cylindrical cavity expansion and contraction in pressure sensitive geomaterials. *Acta Mechanica*, 122:99–122, 1997.

[9] David Durban and M. Baruch. On the problem of a spherical cavity in an infinite elasto-plastic medium. *Journal of Applied Mechanics*, 43:633–638, 1976.

[10] David Durban and N. A. Fleck. Spherical cavity expansion in a drucker-prager solid. *Journal of Applied Mechanics*, 64:743–750, 1997.

[11] David Durban and Rami Masri. Dynamic spherical cavity expansion in a pressure sensitive elastoplastic medium. *International Journal of Solids and Structures*, 41:5697–5716, June 2004.

[12] M. J. Forrestal and V. K. Luk. Dynamic spherical cavity expansion in a compressible elastic-plastic solid. *Journal of Applied Mechanics*, 55:275–279, 1988.

[13] Rodney Hill. *The Mathematical Theory of Plasticity.* Oxford University Press, 1950.

[14] H. G. Hopkins. *Dynamic Expansion of Spherical Cavities in Metals*, volume 1 of *Progress in Solid Mechanics.* North-Holland Publishing Company, Amsterdam, 1960.

[15] S. C. Hunter and R. J. M. Crozier. Similiarity solution for the rapid uniform expansion of a spherical cavity in a compressible elastic-plastic solid. *Quart. Journ. Mech. and Applied Math.*, 21:467–486, 1968.

[16] Rami Masri and David Durban. Dynamic spherical cavity expansion in an elastoplastic compressible mises solid. *Journal of Applied Mechanics*, 72:887–898, November 2005.

[17] Tamer El Sayeda, Alejandro Motaa, Fernando Fraternalib, and Michael Ortiz. Biomechanics of traumatic brain injury. *Computer Methods in Applied Mechanics and Engineering*, 197:46924701, 2008.

[18] G. I. Taylor and H. Quinney. The plastic distortion of metals. *Philosophical Transactions of the Royal Society of London*, 230:323–362, 1932.

[19] Z. Yi, A. K. Agrawal, M. Ettouney, and S. Alampalli. Blast load effects on highway bridges. ii: Failure modes and multihazard correlations. *Journal of Bridge Engineering*, 19(4), 2014.